Chapter 16

Wave Overtopping at Vertical and Steep Structures

Tom Bruce

School of Engineering, University of Edinburgh
King's Buildings, Edinburgh, EH9 3JL, UK
tom.bruce@ed.ac.uk

Jentsje van der Meer

Van der Meer Consulting
P. O. Box 423, 8440 AK Heerenveen, The Netherlands
jm@vandermeerconsulting.nl

Tim Pullen

HR Wallingford
Howbery Park, Wallingford, Oxon, OX10 8BA, UK
tap@hrwallingford.co.uk

William Allsop

HR Wallingford
Howbery Park, Wallingford, Oxon, OX10 8BA, UK
w.allsop@hrwallingford.co.uk

Wave overtopping prediction at vertical structures in earlier days was mainly based on caisson-type structures in relatively deep water. Recent research in many EU-projects has been concentrated on shallower water with waves breaking onto the structure as well. It has led to the definition of two situations: non-impulsive and the most severe impulsive condition. This chapter relies on the *EurOtop* Overtopping Manual, as well as the two previous chapters, 14 and 15, in this handbook. It first describes the mean overtopping discharges for many configurations of vertical and composite vertical structures. Later sections quantify influences such as oblique wave attack, wind effects, model, scale effects, etc.

Individual overtopping volumes are then described. Finally, post-overtopping processes and parameters — landward distribution of discharge; velocities and downfall pressures — are described.

16.1. Introduction

This chapter presents guidance for the assessment of overtopping and post-overtopping processes at vertical and steep-fronted coastal structures such as caisson and blockwork breakwaters and vertical seawalls (see Figs. 16.1 and 16.2). Also included are composite vertical wall structures (where the emergent part of the structure is vertical, fronted by a modest berm) and vertical structures which include a recurve/bull-nose/parapet/wave return wall as the upper part of the defense.

Large vertical breakwaters (Fig. 16.1) are almost universally formed of sand-filled concrete caissons usually resting on a small rock mound. Such caisson breakwaters may reach depths greater than 100 m, under which conditions with no wave breaking at all at the wall would be expected. Conversely, older breakwaters may, out of necessity, have been constructed in shallower water or indeed, built directly on natural rock "skerries." As such, these structures may find themselves exposed to breaking wave, or "impulsive" conditions when the water depth in front of them is

Fig. 16.1. Examples of vertical breakwaters: (left) modern concrete caisson and (right) older structure constructed from concrete blocks.

Fig. 16.2. Examples of vertical seawalls: (left) modern concrete wall and (right) older stone blockwork wall.

sufficiently low. Urban seawalls (e.g., Fig. 16.2) are almost universally fronted by shallow water, and are likely to be exposed to breaking or broken wave conditions, especially in areas of significant tidal range.

There are three principal sources of guidance on this topic preceding this chapter; in the United Kingdom, the Environment Agency's *Overtopping of Seawalls: Design and Assessment Manual*[2]; in the United States, the US Army Corps of Engineers' *Coastal Engineering Manual*[6]; in Japan, Goda's design charts.[11] The guidance presented in this chapter builds upon that of Besley,[2] with adjustments to many formulae based upon further testing since 1999.

For those familiar with Besley,[2] the principal changes/additions are:

- minor adjustments to recommended approach for distinguishing impulsive/non-impulsive conditions (Sec. 16.2);
- all formulae are now given in terms of wave period $T_{m-1,0}$ resulting in an adjusted definition of the h_*, d_*, and V_{bar} parameters (Secs. 16.2.2, 16.2.3, and 16.4.2, respectively) in order to maintain comparability with the earlier work;
- in line with convergence on the $T_{m-1,0}$ measure, formulae using fictitious wave steepness s_{op} have been adjusted to use the new preferred measure $s_{m-1,0}$ (Secs. 16.3.1 and 16.4.2);
- new guidance on mean overtopping under conditions when all waves break before reaching the wall (part of Sec. 16.3.1);
- new guidance on overtopping at vertical walls at zero freeboard (Sec. 16.3.1);
- minor adjustments to formulae for mean overtopping under impulsive conditions due to the availability of additional data, from e.g., the CLASH database[7] (Sec. 16.3.1);
- extension of method for mean overtopping to account for steep (but not vertical) "battered" walls (Sec. 16.3.2);
- new guidance on prediction of mean and wave-by-wave overtopping for oblique wave attack under impulsive conditions (Sec. 16.3.4);
- new guidance on reduction in mean overtopping discharge due to wave return walls/parapets/recurves (Sec. 16.3.5);
- new guidance on the effect of wind on mean overtopping discharge (Sec. 16.3.6);
- inclusion of summary of new evidence on scale effects for laboratory study of overtopping at vertical and steep walls (Sec. 16.3.7);
- new guidance on "post-overtopping" processes, specifically; velocity of "throw"; landward spatial extent of overtopping (Sec. 16.5);
- all formulae are now given explicitly in terms of basic wave and structural parameters without recourse to intermediate definitions of dimensionless overtopping discharge and freeboard parameters specific to impulsive conditions.

The qualitative form of the physical processes occurring when the waves reach the wall are described in Sec. 16.2. Distinctions drawn between different wave/structure "regimes" are reflected in the guidance for assessment of mean overtopping discharges given in Sec. 16.3. The basic assessment tools are presented for plain vertical walls (Sec. 16.3.1), followed by subsections giving advice on how these basic tools should be adjusted to account for other commonly-occurring configurations, such as battered walls (Sec. 16.3.2); vertically composite walls (Sec. 16.3.3);

the effect of oblique wave attack (Sec. 16.3.4); the effect of recurve/wave-return walls (Sec. 16.3.5). The effect of wind is described in Sec. 16.3.6, with scale and model effects reviewed in Sec. 16.3.7. Methods to assess individual "wave-by-wave" overtopping volumes are presented in Sec. 16.4. The current knowledge and advice on post-overtopping processes including velocities, spatial distributions, and post-overtopping loadings are reviewed in Sec. 16.5.

16.2. Wave Processes at Walls

16.2.1. *Overall view*

For assessment of overtopping at steep-fronted and vertical structures the regime of the wave/structure interaction must be identified first, with quite distinct overtopping responses expected for each regime.

On steep walls (vertical, battered, or composite), "non-impulsive" or "pulsating" conditions occur when waves are relatively small in relation to the local water depth, and of lower wave steepnesses. These waves are not critically influenced by the structure toe or approach slope. Overtopping waves run up and over the wall giving rise to (fairly) smoothly-varying loads and "green water" overtopping (Fig. 16.3).

In contrast, "impulsive" conditions (Fig. 16.4) occur on vertical or steep walls when waves are larger in relation to local water depths, perhaps shoaling up over the approach bathymetry or structure toe itself. Under these conditions, some waves will break violently against the wall with (short-duration) forces reaching 10–40 times greater than for non-impulsive conditions. Overtopping discharge under these conditions is characterized by a "violent" uprushing jet of (probably highly aerated) water.

Fig. 16.3. A non-impulsive (pulsating) wave condition at a vertical wall, resulting in a non-impulsive (or "green water") overtopping.

Fig. 16.4. An impulsive (breaking) wave at a vertical wall, resulting in an impulsive (violent) overtopping condition.

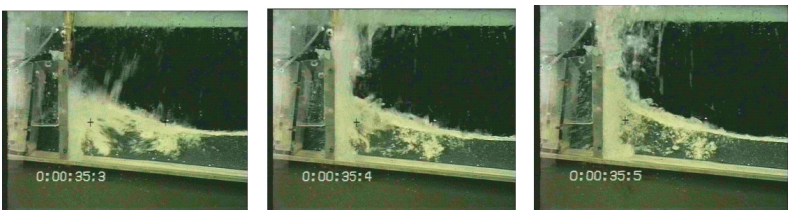

Fig. 16.5. Broken wave at a vertical wall, resulting in a broken wave overtopping condition.

Lying in a narrow band between non-impulsive and impulsive conditions are "near-breaking" conditions where the overtopping is characterized by suddenness and a high-speed, near-vertical up-rushing jet (like impulsive conditions), but where the wave has not quite broken onto the structure and so has not entrained the amount of air associated with fully impulsive conditions. This "near-breaking" condition is also known as the "flip through" condition. This condition gives overtopping in line with impulsive (breaking) conditions and is thus not treated separately.

Many seawalls are constructed at the back of a beach such that breaking waves never reach the seawall, at least not during frequent events where overtopping is of primary importance. For these conditions, particularly for typical shallow beach slopes of less than (say) 1:30, design wave conditions may be given by waves which start breaking (possibly quite some distance) seaward of the wall. These "broken waves" arrive at the wall as a highly-aerated mass of water (Fig. 16.5), giving rise to loadings which show the sort of short-duration peak seen under impulsive conditions (as the leading edge of the mass of water arrives at the wall), but smaller in magnitude due to the high level of aeration.

For cases where the depth at the wall $h_s > 0$, overtopping can be assessed using the method for impulsive conditions. For conditions where the toe of the wall is emergent ($h_s \leq 0$), these methods can no longer be applied and an alternative is required.

In order to proceed with the assessment of overtopping, it is therefore necessary first to determine which is the dominant overtopping regime (impulsive or non-impulsive) for a given structure and design sea state. No single method gives a discriminator which is 100% reliable. The suggested procedure for plain and composite vertical structures includes a transition zone in which there is significant uncertainty in the prediction of dominant overtopping regime, and thus a "worst-case" is taken.

16.2.2. *Overtopping regime discrimination — plain vertical walls*

A method will be described to distinguish between impulsive and non-impulsive conditions at a vertical wall where the toe of the wall is submerged ($h_s > 0$; Fig. 16.6). When the toe of the wall is emergent ($h_s < 0$), only broken waves reach the wall.

For submerged toes ($h_s > 0$), a wave breaking or "impulsiveness" parameter, h_* is defined based on the depth at the toe of the wall, h_s, and incident wave conditions

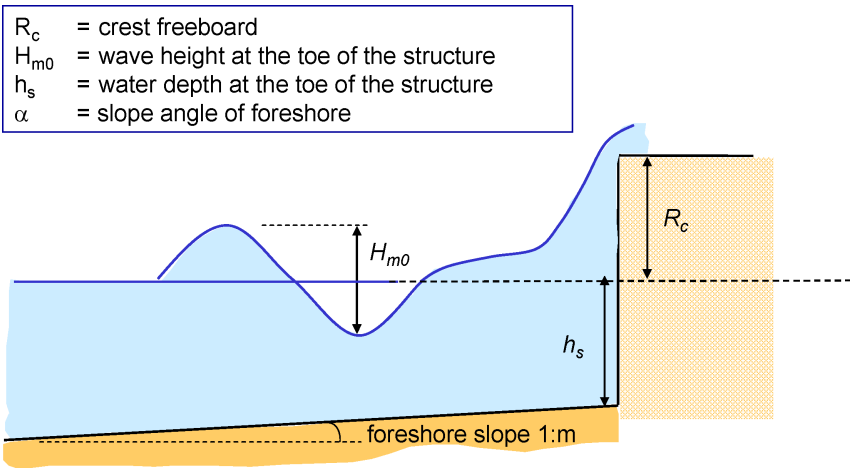

Fig. 16.6. Definition sketch for assessment of overtopping at plain vertical walls.

inshore:

$$h_* = 1.3 \frac{h_s}{H_{m0}} \frac{2\pi h_s}{g T_{m-1,0}^2} \quad \text{or } h_* = \frac{h_s}{H_{m0}} \frac{2\pi h_s}{g T_m^2}, \tag{16.1}$$

where H_{m0} = the significant wave height at the toe of the structure and $T_{m-1,0}$ = the spectral wave period based on spectral moments m_{-1} and m_0, at the same location.

Non-impulsive (pulsating) conditions dominate at the wall when $h_* > 0.3$, and impulsive conditions occur when $h_* < 0.2$. The transition between conditions for which the overtopping response is dominated by breaking and nonbreaking waves lies over $0.2 < h_* < 0.3$. In this region, overtopping should be predicted for both non-impulsive and impulsive conditions, and the larger value assumed.

It should be noted that, for certain long-period waves, $h_* < 0.2$ can be found under conditions for which no breaking at the vertical wall would be expected. Although the term "impulsive overtopping" may not be accurate in these conditions, the overtopping responses nevertheless follow those described by the "impulsive" formulae.

16.2.3. *Overtopping regime discrimination — composite vertical walls*

For vertical composite walls where a berm or significant toe is present in front of the wall, an adjusted version of the method for plain vertical walls should be used (see Fig. 16.7).

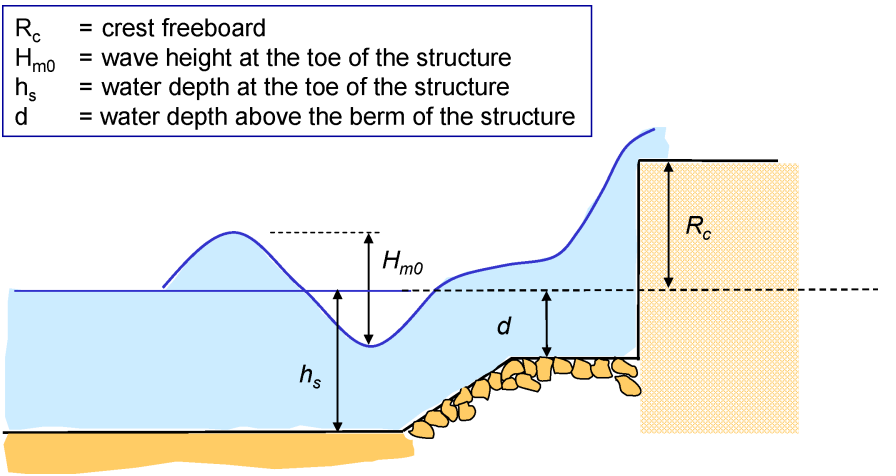

Fig. 16.7. Definition sketch for assessment of overtopping at composite vertical walls.

A modified "impulsiveness" parameter, d_*, is defined in a similar manner to the h_* parameter (for plain vertical walls, Sec. 16.2.2):

$$d_* = 1.3 \frac{d}{H_{m0}} \frac{2\pi h_s}{g T_{m-1,0}^2} \quad \text{or } d_* = \frac{d}{H_{m0}} \frac{2\pi h_s}{g T_m^2}, \tag{16.2}$$

with parameters defined according to Fig. 16.7.

Non-impulsive conditions dominate at the wall when $d_* > 0.3$, and impulsive conditions occur when $d_* < 0.2$. The transition between conditions for which the overtopping response is dominated by breaking and nonbreaking waves lies over $0.2 < d_* < 0.3$. In this region, overtopping should be predicted for both non-impulsive and impulsive conditions, and the larger value assumed.

16.3. Mean Overtopping Discharges for Vertical and Battered Walls

16.3.1. *Plain vertical walls*

This section will give design equations for wave overtopping. The use of these equations may be different, depending on the design process followed. First, an equation is given, which describes the mean of the prediction and the associated uncertainty. This mean prediction should be used for **probabilistic design**, or for prediction of, or comparison with, **measurements**. In the first case, the associated uncertainty as given should be considered, and in the latter case, for instance, 5% upper and lower exceedance curves.

As prediction of wave overtopping is fairly uncertain, the mean prediction should not be used for **deterministic design or safety assessment**. In that case a safety margin should be included in order to account for the uncertainty. Often, this will

be one standard deviation. Each equation will be given as a mean prediction with uncertainty, followed by the application in a deterministic way.

For simple vertical breakwaters, the following equations should be used.

16.3.1.1. *Non-impulsive conditions ($h_* > 0.3$)*

Equation (16.3) gives the mean prediction for non-impulsive conditions and should be used for probabilistic design, or for comparison with measurements. The coefficient of 2.6 for the mean prediction has an associated normal distribution with a standard deviation of $\sigma = 0.4$. This standard deviation can be used to calculate, for instance, 5% exceedance curves. Equation (16.3) has the same shape as equations for smooth and rubble mound slopes (see Chaps. 14 and 15 in this handbook):

$$\frac{q}{\sqrt{gH_{m0}^3}} = 0.04 \exp\left(-2.6 \frac{R_c}{H_{m0}}\right) \quad \text{valid for } 0.1 < R_c/H_{m0} < 3.5. \tag{16.3}$$

Note that a steep (smooth or rubble mound) slope has the same coefficient of 2.6, which means that curves in a log-linear graph will be parallel. For steep slopes, however, the first coefficient is 0.2 and not 0.04, which gives more overtopping. (See also Fig. 16.1 in Chap. 14 of this handbook.)

A well-known formula for vertical walls is given by Allsop *et al.*[1] It is similar to Eq. (16.3) with coefficients 0.05 and 2.78. These coefficients are fairly close to those of Eq. (16.3) with 0.04 and 2.6, and, therefore, this known formula can also be used for simple vertical walls and non-impulsive conditions.

For **deterministic design or safety assessment**, Eq. (16.3) should be used with a coefficient of 2.2 instead of 2.6. Figure 16.8 shows measurements taken from the CLASH database and Eq. (16.3) with a mean prediction, the curve for deterministic design and 5% exceedance curves.

Zero freeboard: For a vertical wall under non-impulsive conditions only one investigation is available,[18] with zero freeboard ($R_c = 0$ or $R_c/H_{m0} = 0$). Figure 16.9 gives the measurements as a function of the fictitious wave steepness. The mean was $q/\sqrt{gH_{m0}^3} = 0.062$ with a standard deviation of $\sigma = 0.006$. The value of 0.062 is slightly larger than the coefficient 0.04 in Eq. (16.3), and even closer to the coefficient of 0.05 of Allsop *et al.*[1] Figure 16.9 shows that the value does not depend on the wave steepness, which is according to Eq. (16.3). For **probabilistic design** or **comparison with measurements**, one can use $q/\sqrt{gH_{m0}^3} = 0.062$ for plain vertical walls with zero freeboard.

For **deterministic design** or **safety assessment**, it is recommended to increase the average overtopping discharge by one standard deviation and use the value of 0.068.

No data are available for impulsive overtopping at zero freeboard at vertical walls.

16.3.1.2. *Impulsive conditions ($h_* < 0.2$)*

The mean prediction for impulsive conditions is given by Eq. (16.4) (Fig. 16.10). The reliability of this equation is described by considering the scatter in the logarithm of

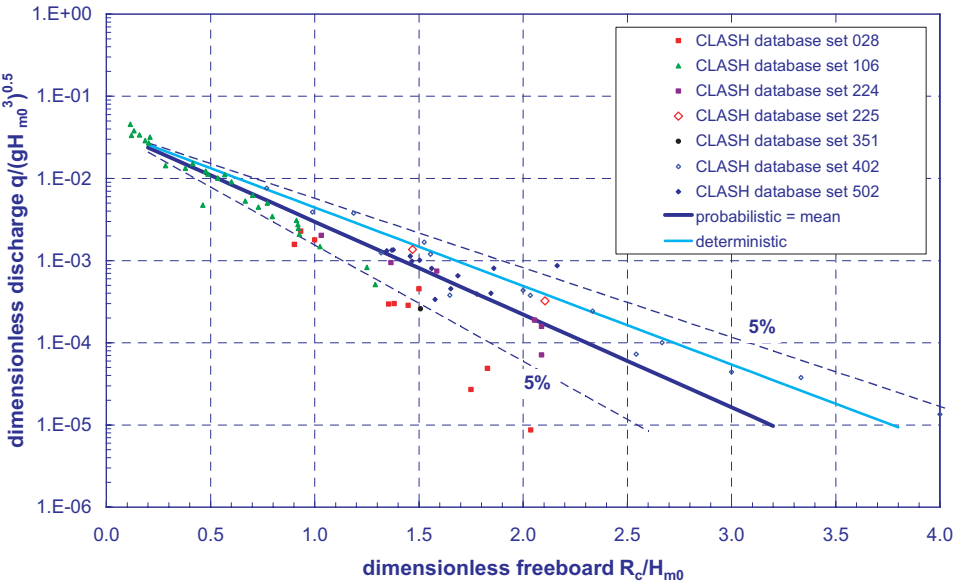

Fig. 16.8. Mean overtopping at a plain vertical wall under non-impulsive conditions [Eq. (16.3)].

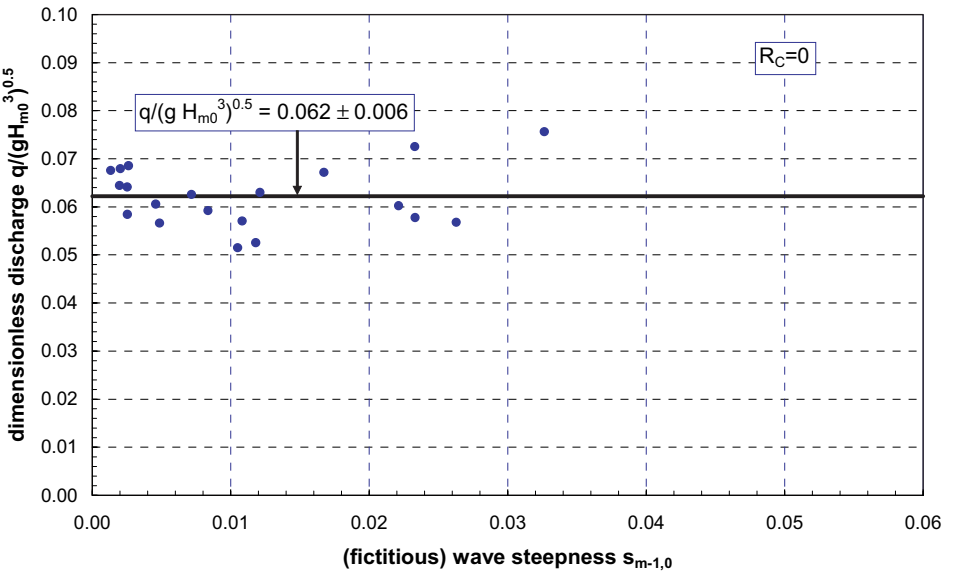

Fig. 16.9. Dimensionless overtopping discharge for zero freeboard.[18]

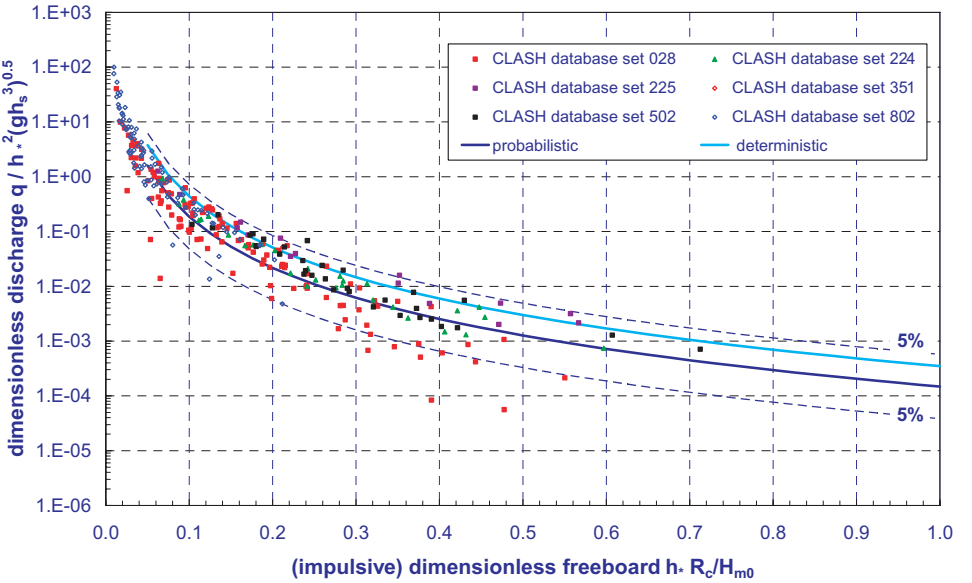

Fig. 16.10. Mean overtopping at a plain vertical wall under impulsive conditions [Eq. (16.4)].

the data about the mean prediction: $\log_{10}(q_{\text{measured}}) - \log_{10}(q_{\text{predicted}})$ is taken as a normally distributed stochastic parameter with a mean of 0 and a standard deviation $\sigma = 0.37$ (i.e., 68% of predictions lie within the range of $\times/\div\, 2.3$). For **probabilistic calculations**, Eq. (16.4) should be taken together with these stochastic coefficients. For predictions of **measurements** or comparison with measurements also Eq. (16.4) should be taken with, for instance, 5% upper and lower exceedance curves. For **deterministic design** or **safety assessment**, a coefficient of 2.8×10^{-4} should be used in Eq. (16.4), instead of 1.5×10^{-4}:

$$\frac{q}{h_*^2\sqrt{gh_s^3}} = 1.5 \times 10^{-4}\left(h_* \frac{R_c}{H_{m0}}\right)^{-3.1} \quad \text{valid over } 0.03 < h_* \frac{R_c}{H_{m0}} < 1.0\,. \tag{16.4}$$

For $h_* R_c/H_{m0} < 0.02$ arising from h_s reducing to very small depths (as opposed to from small relative freeboards), there is evidence supporting an adjustment downward of the predictions of the impulsive formulae due to the observation that only broken waves arrive at the wall.[4] The mean prediction is then described by Eq. (16.5). The reliability of this equation is described by considering the scatter in the logarithm of the data about the mean prediction: $\log_{10}(q_{\text{measured}}) - \log_{10}(q_{\text{predicted}})$ is taken as a normally distributed stochastic parameter with a mean of 0 and a standard deviation $\sigma = 0.15$ (i.e., 68% of predictions lie within the range of $\times/\div\ 1.4$):

$$\frac{q}{h_*^2\sqrt{gh_s^3}} = 2.7 \times 10^{-4}\left(h_* \frac{R_c}{H_{m0}}\right)^{-2.7} \quad \text{valid for } h_* \frac{R_c}{H_{m0}} < 0.02, \quad \text{broken waves.} \tag{16.5}$$

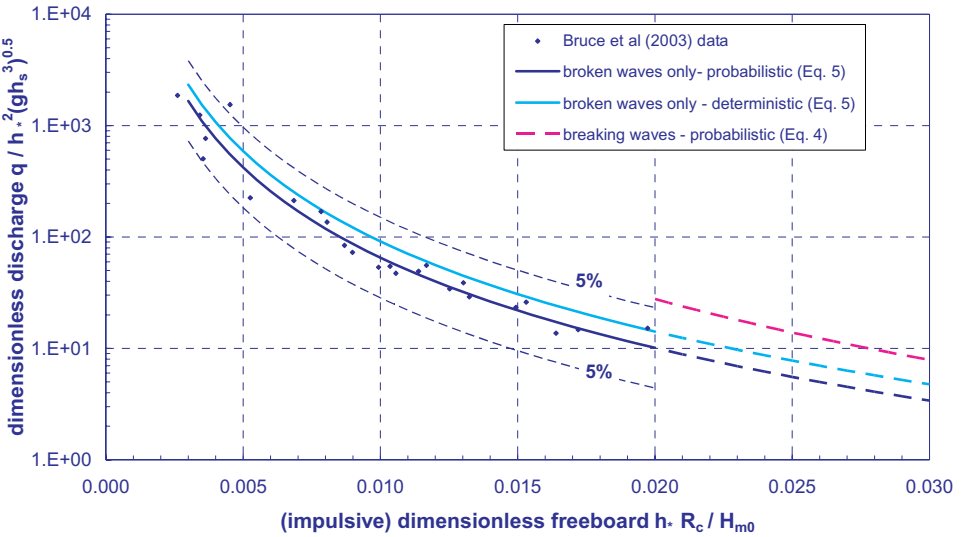

Fig. 16.11. Mean overtopping discharge for lowest $h_* R_c/H_{m0}$ (for broken waves only arriving at wall) with submerged toe ($h_s > 0$). For $0.02 < h_* R_c/H_{m0} < 0.03$, overtopping response is ill-defined — lines for both impulsive conditions (extrapolated to lower $h_* R_c/H_{m0}$) and broken wave only conditions (extrapolated to higher $h_* R_c/H_{m0}$) are shown as dashed lines over this region.

For **probabilistic calculations** or predictions of **measurements** or comparison with measurements, Eq. (16.5) should be taken together with these stochastic coefficients or, for instance, 5% upper and lower exceedance curves. For **deterministic design or safety assessment**, a coefficient of 3.8×10^{-4} should be used in Eq. (16.5), instead of 2.7×10^{-4}.

For $0.02 < h_* R_c/H_{m0} < 0.03$, there appears to be a transition between Eq. (16.4) (for "normal" impulsive conditions) and Eq. (16.5) (for conditions with only broken waves). There is, however, insufficient data upon which to base a firm recommendation in this range. It is suggested that Eq. (16.4) is used down to $h_* R_c/H_{m0} = 0.02$ unless it is clear that only broken waves will arrive at the wall, in which case Eq. (16.5) could be used. Formulae for these low $h_* R_c/H_{m0}$ conditions are shown in Fig. 16.11.

16.3.1.3. *Impulsive conditions, toe emergent ($h_s \leq 0$)*

Data for configurations where the toe of the wall is emergent (i.e., at or above still water level, $h_s \leq 0$) is limited. The only available study suggests an adaptation of a prediction equation for plunging waves on a smooth slope may be used, but particular caution should be exercised in any extrapolation beyond the parameter ranges of the study, which only used a relatively steep ($m = 10$) foreshore slope. This adaptation is given in Eq. (16.6). The reliability of Eq. (16.6) is described by taking the coefficient 2.16 as a normally distributed stochastic parameter with a

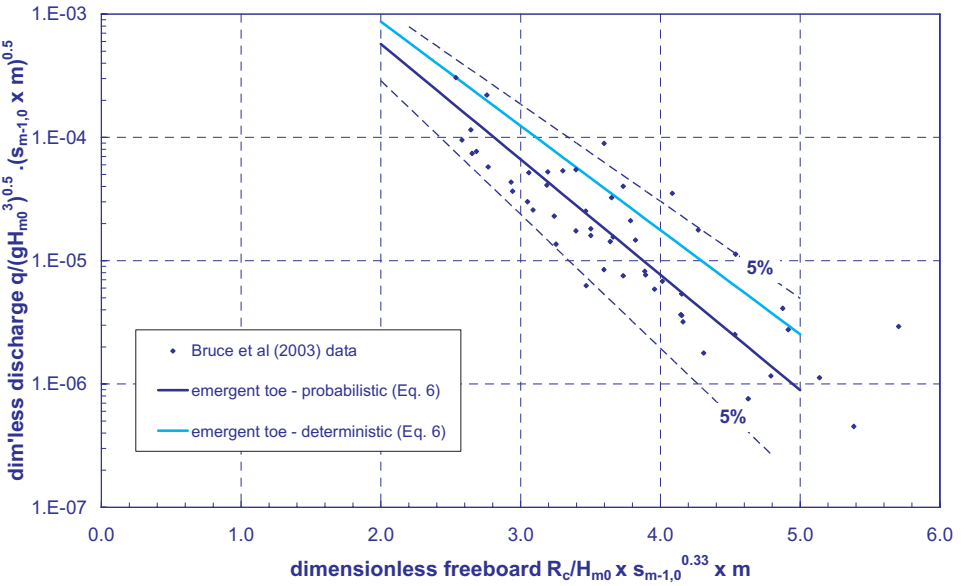

Fig. 16.12. Mean overtopping discharge with emergent toe ($h_s < 0$).

mean of 2.16 and a standard deviation $\sigma = 0.21$:

$$\frac{q}{\sqrt{gH_{m0,\mathrm{deep}}^3}} \cdot \sqrt{m\, s_{m-1,0}} = 0.043 \exp\left(-2.16\, m\, s_{m-1,0}^{0.33} \frac{R_c}{H_{m0,\mathrm{deep}}}\right),$$

valid for

$$2.0 < m\, s_{m-1,0}^{0.33} \frac{R_c}{H_{m0,\mathrm{deep}}} < 5.0; \quad 0.55 \leq R_c/H_{m0,\mathrm{deep}} \leq 1.6; \quad s_{m-1,0} \geq 0.025\,. \tag{16.6}$$

Note: Data only available for $m = 10$ (i.e., 1:10 foreshore slope).

For **deterministic design or safety assessment**, Eq. (16.6) should be used with a coefficient 1.95 instead of 2.16.

Equation (16.6) for overtopping under emergent toe conditions is illustrated in Fig. 16.12. It is emphasized that this formula is based upon a limited dataset of small-scale tests with 1:10 foreshore only and should not be extrapolated outwith the given limits.

16.3.2. *Battered walls*

Near-vertical walls with 10:1 and 5:1 batters are found commonly for older UK seawalls and breakwaters (e.g., Fig. 16.13).

Mean overtopping discharges for battered walls under impulsive conditions are slightly in excess of those for a vertical wall over a wide range of dimensionless

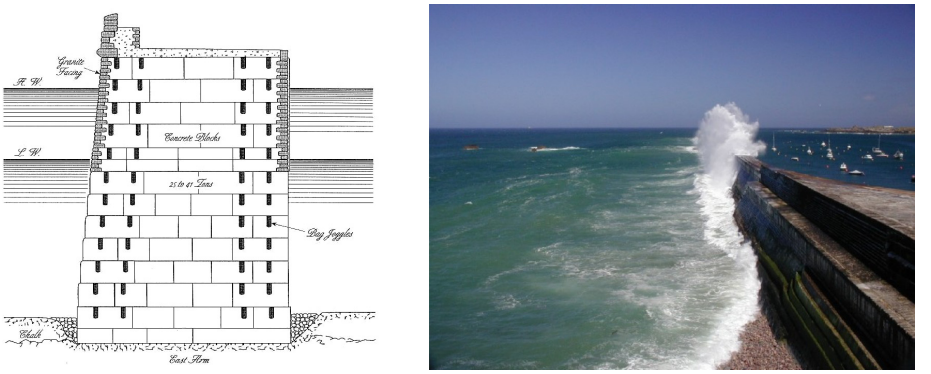

Fig. 16.13. Battered walls: typical cross-section (left), and Admiralty Breakwater, Alderney Channel Islands (right, courtesy G. Müller).

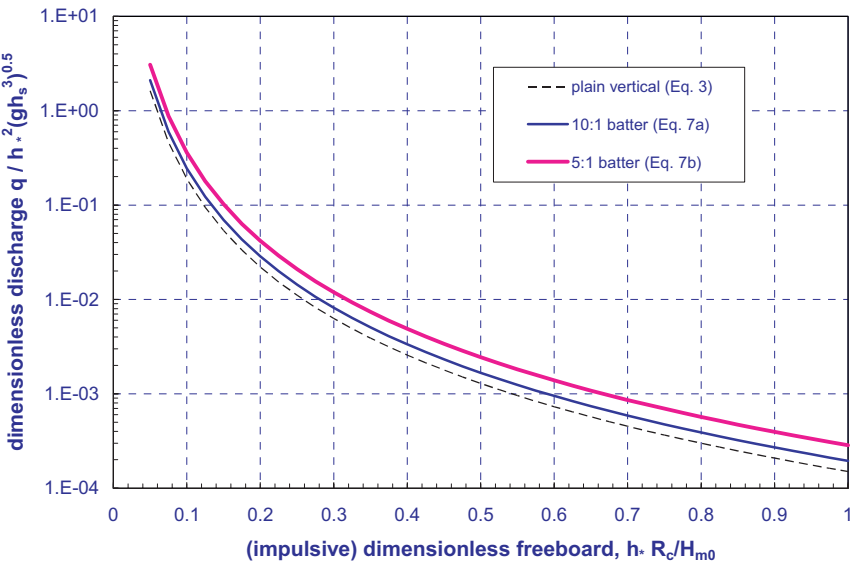

Fig. 16.14. Overtopping for a 10:1 and 5:1 battered walls.

freeboards. Multiplying factors are given in Eqs. (16.17a) and (16.7b) (plotted in Fig. 16.14).

$$\text{10:1 battered wall:} \qquad q_{10:1\text{batter}} = q_{\text{vertical}} \times 1.3\,, \tag{16.7a}$$

$$\text{5:1 battered wall:} \qquad q_{5:1\text{batter}} = q_{\text{vertical}} \times 1.9\,, \tag{16.7b}$$

where q_{vertical} is arrived at from Eq. (16.4). The uncertainty in the final estimated overtopping discharge can be estimated as per the plain vertical cases.

No dataset is available to indicate an appropriate adjustment under non-impulsive conditions. An alternative method, however, may be to calculate

overtopping for a vertical structure and for a steep smooth slope 1:1. By using the $\cot\alpha$ of the battered wall as the parameter (between the limits 0 and 1), a fair guess will be reached (see also Fig. 14.2 in Chap. 14 of this handbook).

16.3.3. *Composite vertical walls*

It is well established that a relatively small toe berm can change wave-breaking characteristics, thus substantially altering the type and magnitude of wave loadings. Many vertical seawalls may be fronted by rock mounds with the intention of protecting the toe of the wall from scour. The toe configuration can vary considerably, potentially modifying the overtopping behavior of the structure. Three types of mounds can be identified:

(i) Small toe mounds which have an insignificant effect on the waves approaching the wall — here, the toe may be ignored and calculations proceed as for simple vertical (or battered) walls.
(ii) Moderate mounds, which significantly affect wave-breaking conditions, but are still below water level. Here, a modified approach is required.
(iii) Emergent mounds in which the crest of the armor protrudes above still water level. Prediction methods for these structures may be adapted from those for crown walls on a rubble mound (Chap. 15 of this handbook).

For assessment of mean overtopping discharge at a composite vertical seawall or breakwater, the overtopping regime (impulsive/non-impulsive) must be determined (see Sec. 16.2.3).

When non-impulsive conditions prevail, overtopping can be predicted by the standard method given previously for non-impulsive conditions at plain vertical structures [Eq. (16.3)].

For conditions determined to be impulsive, a modified version of the impulsive prediction method for plain vertical walls is recommended, accounting for the presence of the mound by use of d and d_*.

16.3.3.1. *Impulsive conditions ($d_* \leq 0.2$)*

The mean prediction for impulsive conditions at a composite vertical structure is given by Eq. (16.8), and Fig. 16.15. The reliability of this equation is described by considering the scatter *in the logarithm* of the data about the mean prediction: $\log_{10}(q_{\text{measured}}) - \log_{10}(q_{\text{predicted}})$ is taken as a normally distributed stochastic parameter with a mean of 0 and a standard deviation $\sigma = 0.28$ (i.e., 68% of predictions lie within the range of $\times/\div 1.9$). For **probabilistic calculations**, Eq. (16.8) should be taken together with these stochastic coefficients:

$$\frac{q}{d_*^2\sqrt{gd^3}} = 4.1 \times 10^{-4}\left(d_*\frac{R_c}{H_{m0}}\right)^{-2.9},$$

valid for

$$0.05 < d_*\frac{R_c}{H_{m0}} < 1.0 \quad \text{and} \quad h_* < 0.3\,. \tag{16.8}$$

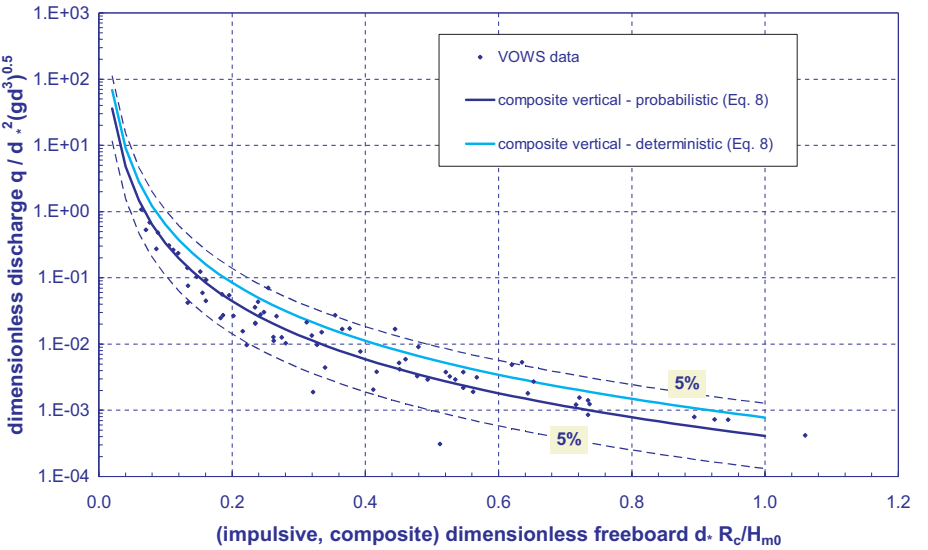

Fig. 16.15. Overtopping for composite vertical walls.

For **deterministic design or safety assessment**, Eq. (16.8) should be used with a coefficient of 7.8×10^{-4}, instead of 4.1×10^{-4}, and an exponent of -2.6 instead of -2.9.

16.3.4. *Effect of oblique waves*

Seawalls and breakwaters seldom align perfectly with incoming waves. The assessment methods presented thus far are only valid for shore-normal wave attack. In this subsection, advice is given on how the methods for shore-normal wave attack (obliquity $\beta = 0°$) should be adjusted for oblique wave attack. As for zero obliquity, overtopping response depends critically upon the physical form (or "regime") of the wave/wall interaction — non-impulsive, impulsive, or broken. As such, the first step is to use the methods given in Sec. 16.2 to determine the form of overtopping for shore-normal (zero obliquity). Based upon the outcome of this, guidance under "non-impulsive conditions" or "impulsive conditions" should be followed.

For **non-impulsive conditions**, an adjusted version of Eq. (16.3) should be used:

$$\frac{q}{\sqrt{gH_{m0}^3}} = 0.04 \exp\left(-\frac{2.6}{\gamma_\beta}\frac{R_c}{H_{m0}}\right), \tag{16.9}$$

where γ_β is the reduction factor for angle of attack and is given by

$$\begin{aligned} \gamma_\beta &= 1 - 0.0062\beta \quad \text{for } 0^0 < \beta < 45°\,, \\ \gamma_\beta &= 0.72 \quad \text{for } \beta \geq 45°\,, \end{aligned} \tag{16.10}$$

and β is the angle of attack relative to the normal, in degrees.

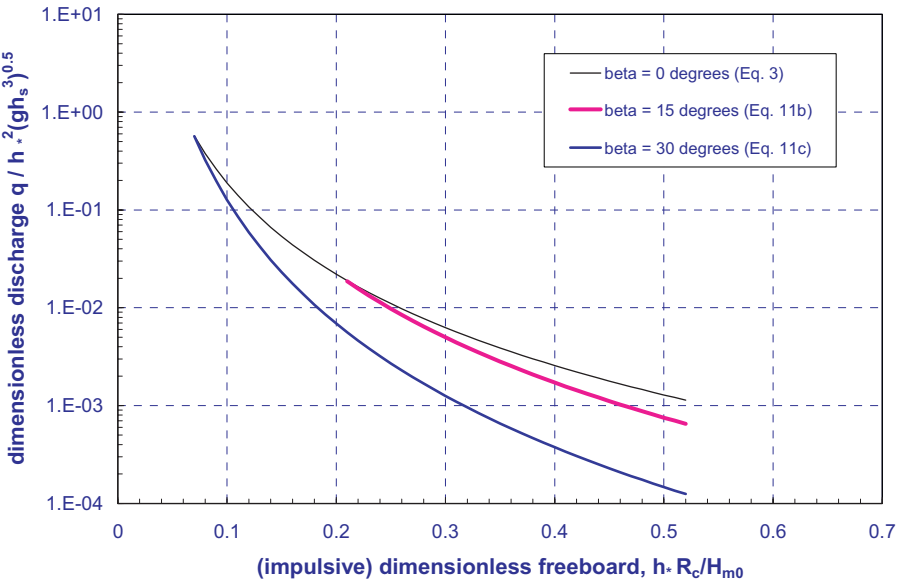

Fig. 16.16. Overtopping of vertical walls under oblique wave attack.

For conditions that would be identified as **impulsive** for normal ($\beta = 0°$) wave attack, a more complex picture emerges.[13] Diminished incidence of impulsive overtopping is observed with increasing obliquity (angle β) of wave attack (Fig. 16.16). This results not only in reductions in mean discharge with increasing β, but also, for $\beta \geq 60°$, a switch back over to the functional form observed for non-impulsive conditions [i.e., a move away from a power-law decay such as Eq. (16.4) to an exponential one such as Eq. (16.3)].

The mean predictions are given by Eqs. (16.11a)–(16.11d). Data only exist for the discrete values of obliquity listed:

$$\text{for } \beta = 15°,\ h_* \frac{R_c}{H_{m0}} \geq 0.2, \quad \frac{q}{h_*^2 \sqrt{g h_s^3}} = 5.8 \times 10^{-5} \left(h_* \frac{R_c}{H_{m0}} \right)^{-3.7}, \tag{16.11a}$$

$$\text{for } \beta = 15°,\ h_* \frac{R_c}{H_{m0}} < 0.2, \quad \text{as per impulsive } \beta = 0° (\text{Eq. } 16.4), \tag{16.11b}$$

$$\text{for } \beta = 30°,\ h_* \frac{R_c}{H_{m0}} \geq 0.07, \quad \frac{q}{h_*^2 \sqrt{g h_s^3}} = 8.0 \times 10^{-6} \left(h_* \frac{R_c}{H_{m0}} \right)^{-4.2}, \tag{16.11c}$$

$$\text{for } \beta = 60°,\ h_* \frac{R_c}{H_{m0}} \geq 0.07, \quad \text{as per non-impulsive } \beta = 60° (\text{Eq. } 16.10). \tag{16.11d}$$

Significant spatial variability of overtopping volumes along the seawall under oblique wave attack are observed/measured in physical model studies. For **deterministic design**, Eqs. (16.12a)–(16.12c) should be used, as these give estimates of

the "worst case" conditions at locations along the wall where the discharge is the greatest:

$$\text{for } \beta = 15^0,\ h_* \frac{R_c}{H_{m0}} \geq 0.2, \quad \text{as per impulsive } \beta = 0^\circ \text{ (Eq. 16.4)}, \tag{16.12a}$$

$$\text{for } \beta = 30^0,\ h_* \frac{R_c}{H_{m0}} \geq 0.07, \quad \text{as per impulsive } \beta = 15^\circ \text{ (Eq. 16.11b)}, \tag{16.12b}$$

$$\text{for } \beta = 60^0,\ h_* \frac{R_c}{H_{m0}} \geq 0.07, \quad \text{as per non-impulsive } \beta = 0^\circ \text{ (Eq. 16.3)}. \tag{16.12c}$$

16.3.5. *Effect of bullnose and recurve walls*

Designers of vertical seawalls and breakwaters have often included some form of seaward overhang (recurve/parapet/wave return wall/bullnose) as a part of the structure with the design motivation of reducing wave overtopping by deflecting back seaward uprushing water (e.g., Figs. 16.17 and 16.18). The mechanisms determining the effectiveness of a recurve are complex and not yet fully described. The guidance presented here is based upon physical model studies.[12,15]

Parameters for the assessment of overtopping at structures with bullnose/recurve walls are shown in Fig. 16.19.

Two conditions are distinguished:

- the familiar case of the parapet/bullnose/recurve overhanging seaward ($\alpha < 90^\circ$), and

Fig. 16.17. An example of a modern, large vertical breakwater with wave return wall (left) and cross-section of an older seawall with recurve (right).

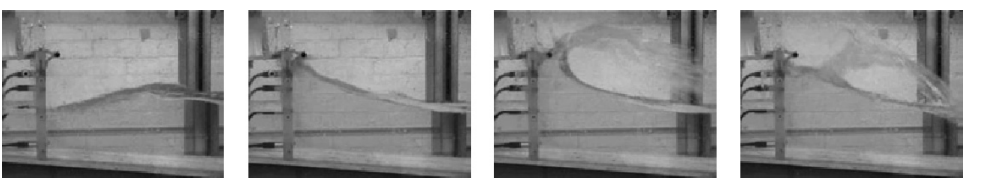

Fig. 16.18. A sequence showing the function of a parapet/wave return wall in reducing overtopping by redirecting the uprushing water seaward (back to right).

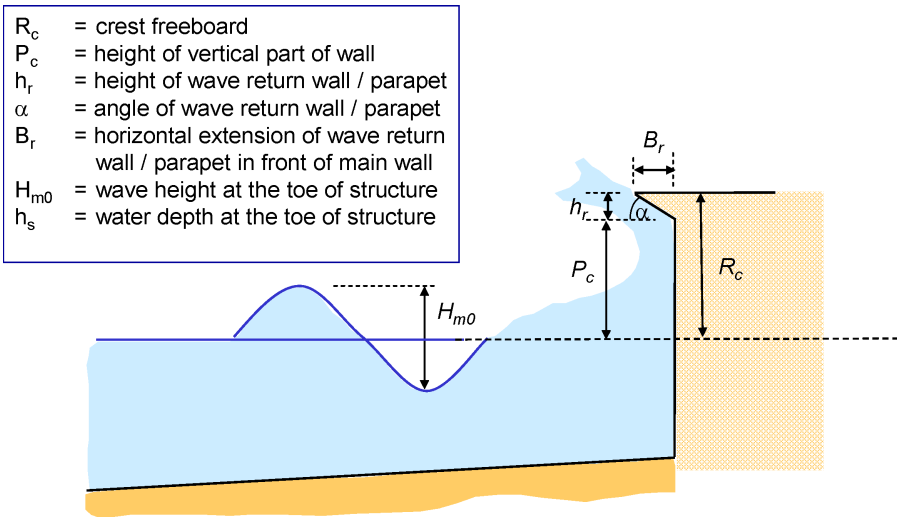

Fig. 16.19. Parameter definitions for assessment of overtopping at structures with parapet/wave return wall.

- the case where a wall is chamfered backward at the crest [normally admitting *greater* overtopping ($\alpha > 90°$)].

For the latter, chamfered wall case, influence factors γ should be applied to Franco *et al.*'s equation[10] for non-impulsive mean discharge [Eq. (16.13)] with the value of γ selected as shown[8]:

$$\frac{q}{(gH_{m0}^3)^{0.5}} = 0.2 \exp\left(-\frac{4.3}{\gamma}\frac{R_c}{H_{m0}}\right), \tag{16.13}$$

$$\gamma = 1.01 \quad \text{for } \alpha = 120°,$$
$$\gamma = 1.13 \quad \text{for } \alpha = 135°,$$
$$\gamma = 1.07 \quad \text{for } \alpha = 150°.$$

For the familiar case of overhanging parapet/recurve/bullnose, the effectiveness of the recurve/parapet in reducing overtopping is quantified by a factor k defined as

$$k = \frac{q_{\text{with\_recurve}}}{q_{\text{without\_recurve}}}. \tag{16.14}$$

The decision chart in Fig. 16.20 can then be used to arrive at a value of k, which in turn can be applied by multiplication to the mean discharge predicted by the most appropriate method for the plain vertical wall (with the same R_c, h_s, etc.). The decision chart shows three levels of decision:

- whether the parapet is angled seaward or landward;
- if seaward ($\alpha < 90°$), whether conditions are in the small (left box), intermediate (middle box), or large (right box) reduction regimes;

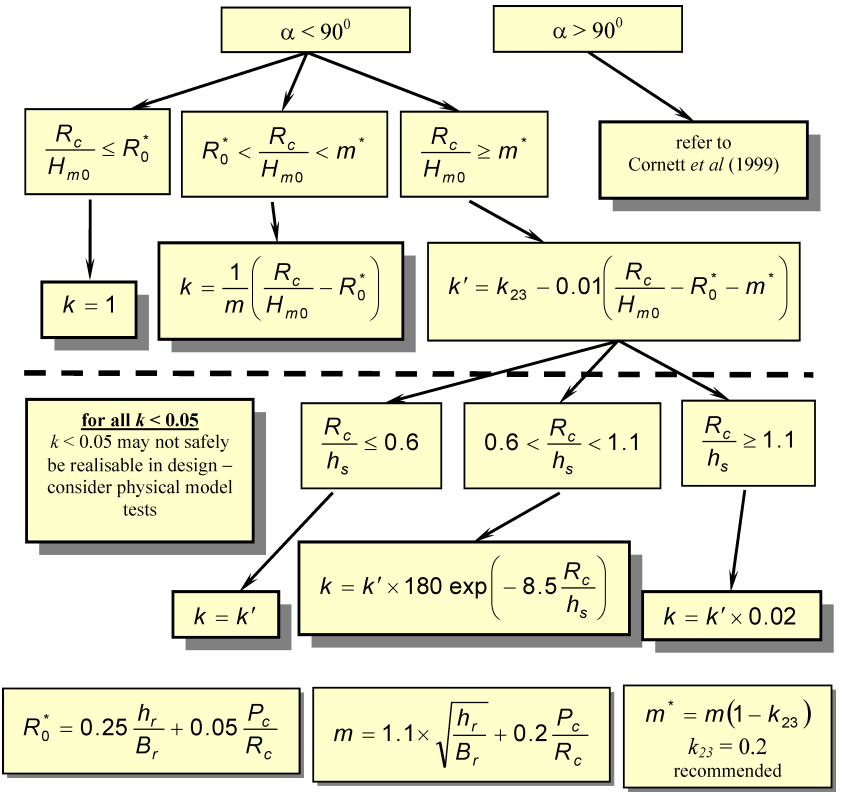

Fig. 16.20. "Decision chart" summarizing methodology for tentative guidance. Note that symbols R_0^*, k_{23}, m, and m^* used (only) at intermediate stages of the procedure are defined in the lowest boxes in the figure. Please refer to text for further explanation.

- if in the regime of largest reductions (greatest parapet effectiveness; $R_c/H_{m0} \geq R_0^* + m^*$), which of the three further subregimes (for different R_c/h_s) is appropriate.

Given the level of scatter in the original data and the observation that the methodology is not securely founded on the detailed physical mechanisms/processes, it is suggested that it is impractical to design for $k < 0.05$, i.e., reductions in mean discharges by factors greater than 20 cannot be predicted with confidence. If such large (or larger) reductions are required, a detailed physical model study should be considered.

16.3.6. *Effect of wind*

Wind may affect overtopping processes and thus discharges by

(1) changing the shape of the incident wave crest at the structure resulting in a possible modification of the dominant regime of wave interaction with the wall;

(2) blowing up-rushing water over the crest of the structure (for an onshore wind, with the reverse effect for an offshore wind) resulting in possible modification of mean overtopping discharge and wave-by-wave overtopping volumes;
(3) modifying the physical form of the overtopping volume or jet, especially in terms of its aeration and breakup resulting in possible modification to post-overtopping characteristics such as throw speed, landward distribution of discharge, and any resulting post-overtopping loadings (e.g., downfall pressures).

The modeling of any of these effects in small-scale laboratory tests presents very great difficulties owing to fundamental barriers to the simultaneous scaling of the wave-structure and water–air interaction processes. Very little information is available to offer guidance on effect (1) — the reshaping of the incident waves. Comparisons of laboratory and field data (both with and without wind) have enabled some upper (conservative) bounds to be placed upon effect (2) — the intuitive wind-assistance in "pushing" of up-rushing water landward across the crest. These are discussed immediately below. Discussion of effect (3) — modification to "post-overtopping" processes — is reserved for Secs. 16.5.3 and 16.5.4 (on distributions and downfalling pressures, respectively).

Several investigations on vertical structures have suggested different adjustment factors f_{wind} ranging from 30% to 40% to up to 300% (Fig. 16.21) either using a paddle wheel or large fans to transport uprushing water over the wall.

When these tests were revisited, a simple adjustment factor was proposed for the mean discharge based upon small-scale tests q_{ss}, which is already scaled up by

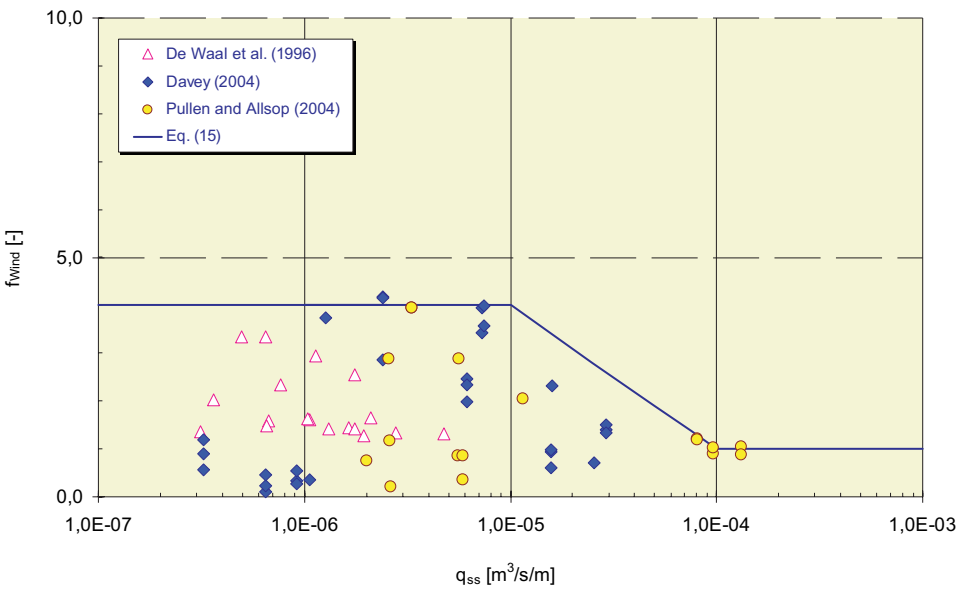

Fig. 16.21. Wind adjustment factor f_{wind} plotted over mean overtopping rates q_{ss} for three datasets.

appropriate scaling to full-scale (see also Ref. 9):

$$f_{\text{wind}} = \begin{cases} 4.0 & \text{for } q_{ss} \leq 10^{-5}\,\text{m}^3/\text{s/m} \\ 1.0 + 3 \cdot (-\log q_{ss} - 4) & \text{for } 10^{-5} < q_{ss} < 10^{-4}\,\text{m}^3/\text{s/m} \\ 1.0 & \text{for } q_{ss} \geq 10^{-4}\,\text{m}^3/\text{s/m}\,. \end{cases} \tag{16.15}$$

From Eq. (16.15), it becomes clear that the influence of wind only gets important for very low overtopping rates below $q_{ss} = 0.1\,\text{l/s/m}$. Hence, in many practical cases, the influence of wind may be disregarded. The mean overtopping discharge including wind becomes

$$q_{\text{with wind}} = f_{\text{wind}} \times q_{ss}\,. \tag{16.16}$$

16.3.7. *Scale and model effect corrections*

Tests in a large-scale wave channel (Fig. 16.22) and field measurements (Fig. 16.23) have demonstrated that with the exception of wind effect (Sec. 16.3.6), results of overtopping measurements in small-scale laboratory studies may be securely scaled to full-scale under non-impulsive and impulsive overtopping conditions.[16,17]

No information is yet available on the scaling of small-scale data under conditions where broken wave attack dominates. Comparison of measurements of wave loadings on vertical structures under broken wave attack at small scale and in the field suggests that prototype loadings will be *over-estimated* by small scale tests in the presence of highly-aerated broken waves. Thus, although the methods presented for

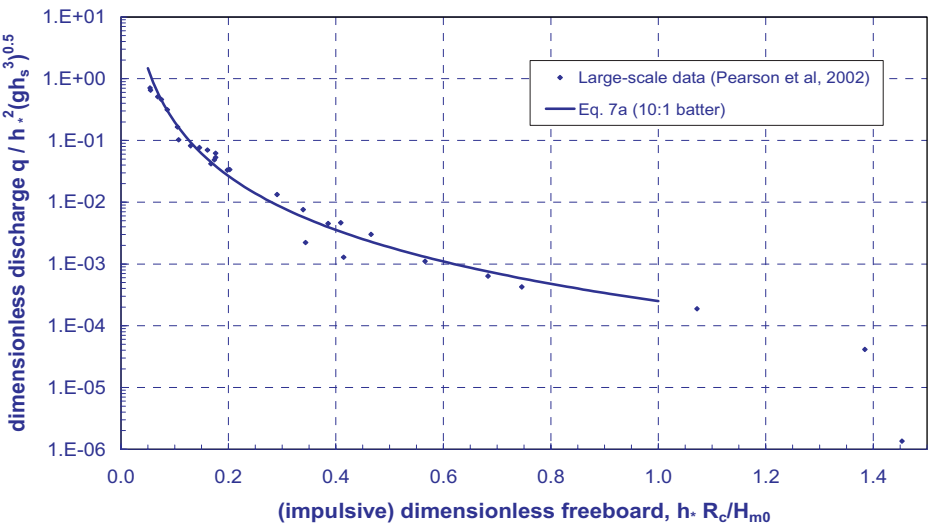

Fig. 16.22. Large-scale laboratory measurements of mean discharge at 10:1 battered wall under impulsive conditions showing agreement with prediction line based upon small-scale tests [Eq. (16.7a)].

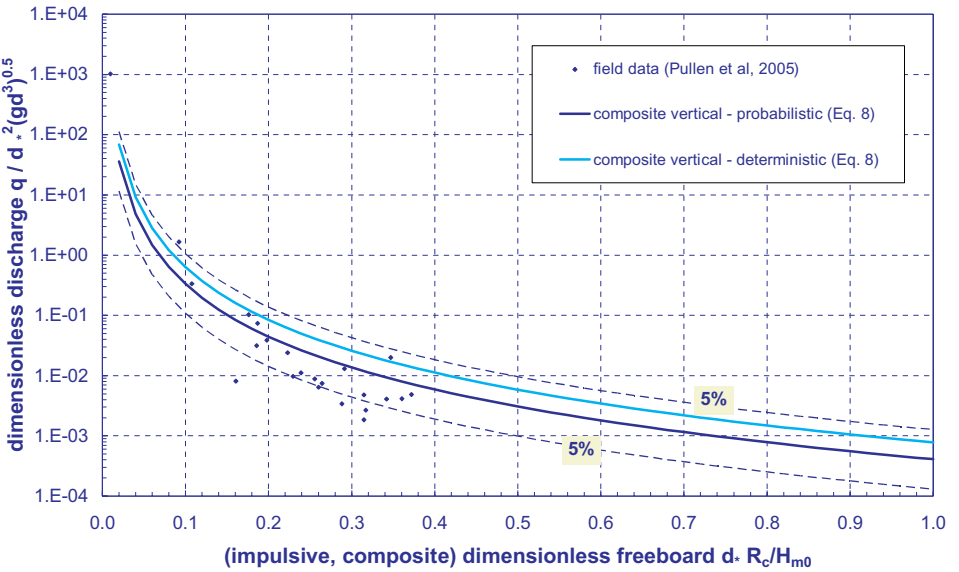

Fig. 16.23. Results from field measurements of mean discharge at Samphire Hoe, UK, plotted together with Eq. (16.8).

the assessment of overtopping discharges under broken wave conditions given in Sec. 16.3.1 have not been verified at large scale or in the field, any scale correction is expected to give a *reduction* in the predicted discharge.

16.4. Overtopping Volumes

16.4.1. *Introduction*

While the prediction of mean discharge (Sec. 16.3) offers the information required to assess whether overtopping is slight, moderate, or severe, and make a link to any possible flooding that might result, the prediction of the volumes associated with individual wave events can offer an alternative (and often more appropriate) measure for the assessment of tolerable overtopping levels and possible direct hazard. First, a method is given for the prediction of maximum overtopping volumes expected associated with individual wave events for plain vertical structures under perpendicular wave attack (Sec. 16.4.2). This method is then extended to composite (bermed) structures (Sec. 16.4.3) and to conditions of oblique wave attack (Sec. 16.4.4). Finally, a short section on scale effects is included (Sec. 16.4.5).

The methods given for perpendicular wave attack are the same as those given previously in UK guidance,[2] but now using the $T_{m-1,0}$ period measure (with Weibull parameters, steepness values, etc., adjusted accordingly). The extension to oblique wave attack is new.

16.4.2. *Overtopping volumes at plain vertical walls*

The first step in the estimation of a maximum expected individual wave overtopping volume is to estimate the number of waves overtopping (N_{ow}) in a sequence of N_w incident waves.

For **non-impulsive conditions**, this was found to be well described by Franco *et al.*,[10] as follows:

$$N_{ow} = N_w \exp\left\{-1.21\left(\frac{R_c}{H_{m0}}\right)^2\right\} \quad (\text{for } h_* > 0.3)\,. \tag{16.17}$$

Under **impulsive conditions**, N_{ow} is better described by[2]

$$N_{ow} = 0.031\, N_w \times \frac{H_{m0}}{h_*\, R_c} \quad (\text{for } h_* < 0.3)\,. \tag{16.18}$$

The distribution of individual overtopping volumes in a sequence is generally well described by a two-parameter Weibull distribution (see also Chap. 14, Sec. 14.2.2 of this handbook):

$$P_V = 1 - \exp\left\{-\left(\frac{V}{a}\right)^b\right\}, \tag{16.19}$$

where P_V is the probability that an individual event volume will not exceed V; a and b are Weibull "shape" and "scale" parameters, respectively. Thus, to estimate the largest event in a wave sequence predicted to include (e.g.) $N_{ow} = 200$ overtopping events, $V_{\max}$ would be found by taking $P_V = 1/200 = 0.005$. Equation (16.19) can then be rearranged to give

$$V_{\max} = a\,(\ln N_{ow})^{1/b}\,. \tag{16.20}$$

The Weibull shape parameter a depends upon the average volume per overtopping wave V_{bar}, where

$$V_{\text{bar}} = 0.8\frac{qT_{m-1,0}\,N_w}{N_{ow}} \quad \text{or} \quad V_{\text{bar}} = \frac{qT_m\,N_w}{N_{ow}}\,. \tag{16.21}$$

For **non-impulsive conditions**, there is a weak steepness-dependency for the scale and shape parameters a and b:

$$a = \begin{cases} 0.74V_{\text{bar}} \\ 0.90V_{\text{bar}} \end{cases} \quad b = \begin{cases} 0.66 & \text{for } s_{m-1,0} = 0.024 \\ 0.82 & \text{for } s_{m-1,0} = 0.048 \end{cases} \quad \text{for } h_* > 0.3\,. \tag{16.22}$$

(Note that the fictitious steepness values $s_{m-1,0} = 0.024$ and 0.048 in Eq. (16.22) correspond to the values of $s_{\text{op}} = 0.02$ and 0.04 quoted by Besley[2].)

For **impulsive conditions**[2,16]:

$$a = 0.92V_{\text{bar}}, \quad b = 0.85 \qquad \text{for } h_* < 0.3\,. \tag{16.23}$$

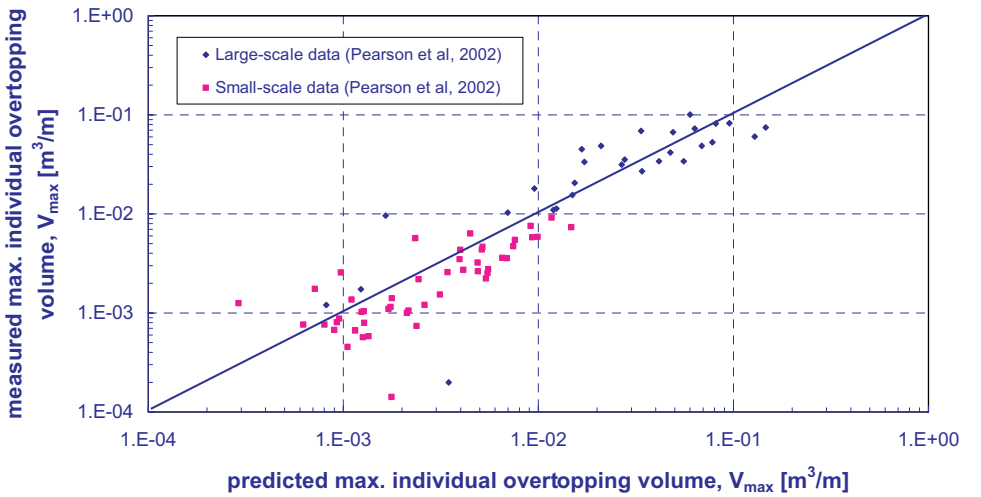

Fig. 16.24. Predicted and measured maximum individual overtopping volume — small- and large-scale tests.[16]

The effectiveness of the predictor under impulsive conditions can be gauged from Fig. 16.24. Note that all the a values are fairly similar, leading to similar steep distributions (see also Sec. 14.2.2 in Chap. 14 of this handbook). A further step in development could be to choose a fixed value for a and modify b accordingly.

16.4.3. *Overtopping volumes at composite (bermed) structures*

There is very little information available specifically addressing wave-by-wave overtopping volumes at composite structures. The guidance offered by Besley[2] remains the best available. No new formulae or Weibull a, b values are known; so, for the purposes of maximum overtopping volume prediction, the methods for plain vertical walls (Sec. 16.4.2) are used. The key discriminator is that composite structures whose mound is sufficiently small to play little role in the overtopping process are treated as *plain vertical, non-impulsive*, whereas those with large mounds are treated as *plain vertical, impulsive*.

For this purpose, the significance of the mound is assessed using the "impulsiveness" parameter for composite structures, d_* [Eq. (16.2)]. "Small mound" is defined as $d_* > 0.3$, with $d_* < 0.3$ being "large mound."

16.4.4. *Overtopping volumes at plain vertical walls under oblique wave attack*

For *non-impulsive* conditions, an adjusted form of Eq. (16.17) is suggested[10]:

$$N_{ow} = N_w \exp\left\{-\frac{1}{C^2}\left(\frac{R_c}{H_{m0}}\right)^2\right\} \quad \text{for } h_* > 0.3\,. \tag{16.24}$$

Table 16.1. Summary of prediction formulae for individual overtopping volumes under oblique wave attack. Oblique cases valid for $0.2 < h_* R_c/H_{m0} < 0.65$. For $0.07 < h_* R_c/H_{m0} < 0.2$, the $\beta = 0^0$ formulae should be used for all β.

$\beta = 15°$	$\beta = 30°$	$\beta = 60°$
$N_{ow} = 0.01\ N_w \times \left(\frac{H_{m0}}{h_* R_c}\right)^{-1.6}$	$N_{ow} = 0.01\ N_w \times \left(\frac{H_{m0}}{h_* R_c}\right)^{-1.4}$	Treat as non-impulsive
$a = 1.06\ V_{\text{bar}}$	$a = 1.04\ V_{\text{bar}}$	Treat as non-impulsive
$b = 1.18$	$b = 1.27$	Treat as non-impulsive

C is given by

$$C = \begin{cases} 0.91 & \text{for } \beta = 0° \\ 0.91 - 0.00425\beta & \text{for } 0° < \beta < 40° \\ 0.74 & \text{for } \beta \geq 40° \end{cases} \quad \text{for } h_* > 0.3\,. \tag{16.25}$$

For *impulsive conditions* (as determined for perpendicular i.e., $\beta = 0°$ wave attack), the procedure is the same as for perpendicular ($\beta = 0°$) wave attack, but different formulae should be used for estimating the number of overtopping waves (N_{ow}) and Weibull shape and scale parameters (Table 16.1).[13]

16.4.5. *Scale effects for individual overtopping volumes*

Measurements from large-scale laboratory tests indicate that formulae for overtopping volumes, based largely upon small-scale physical model studies, scale well (Fig. 16.24).[16] No data from the field is available to support "scale-ability" from large-scale laboratory scales to prototype conditions.

16.5. Overtopping Velocities, Distributions, and Down-Fall Pressures

16.5.1. *Introduction to post-overtopping processes*

There are many design issues for which knowledge of just the mean and/or wave-by-wave overtopping discharges/volumes are not sufficient, e.g.,

- assessment of direct hazard to people, vehicles, and buildings in the zone immediately landward of the seawall;
- assessment of potential for damage to elements of the structure itself (e.g., crown wall, crown deck, secondary defenses).

The appreciation of the importance of being able to predict more than overtopping discharges and volumes has led to significant advances in the description and quantification of what can be termed "post-overtopping" processes, specifically, the current state of prediction tools for:

- the speed of an overtopping jet (or "throw velocity"),
- the spatial extent reached by (impulsive) overtopping volumes, and

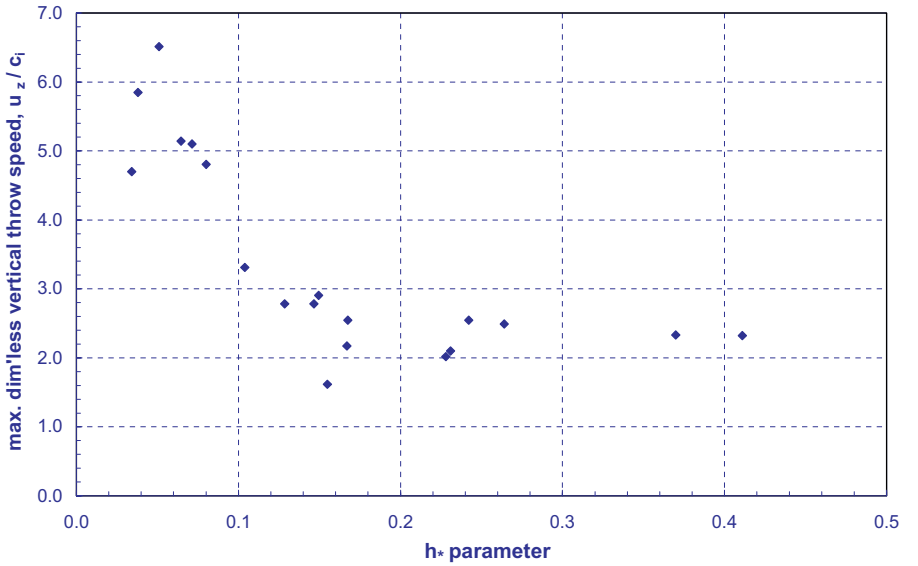

Fig. 16.25. Speed of upward projection of overtopping jet past structure crest plotted with h_* parameter (after Bruce *et al.*[5]).

- the pressures that may arise due to the downfalling overtopped jet impacting on the structure's crown deck.

16.5.2. *Overtopping throw speeds*

Studies at small scale, based upon video footage suggest that the vertical speed with which the overtopping jet leaves the crest of the structure (u_z) may be estimated as (Fig. 16.25):

$$u_z \approx \begin{cases} 2 \text{ to } 2.5 \times c_i & \text{for non-impulsive conditions}, \\ 5 \text{ to } 7 \times c_i & \text{for impulsive conditions}, \end{cases} \tag{16.26}$$

where $c_i = \sqrt{gh_s}$ is the inshore wave celerity.[5]

16.5.3. *Spatial extent of overtopped discharge*

The spatial distribution of overtopped discharge may be of interest in determining zones affected by direct wave overtopping hazard (to people, vehicles, buildings close behind the structure crest, or to elements of the structure itself).

Under green water (non-impulsive) conditions, the distribution of overtopped water will depend principally on the form of the area immediately landward of the structure's crest (slopes, drainage, obstructions, etc.) and no generic guidance can be offered (though, see Sec. 16.5.2 for information on speeds of overtopping jets).

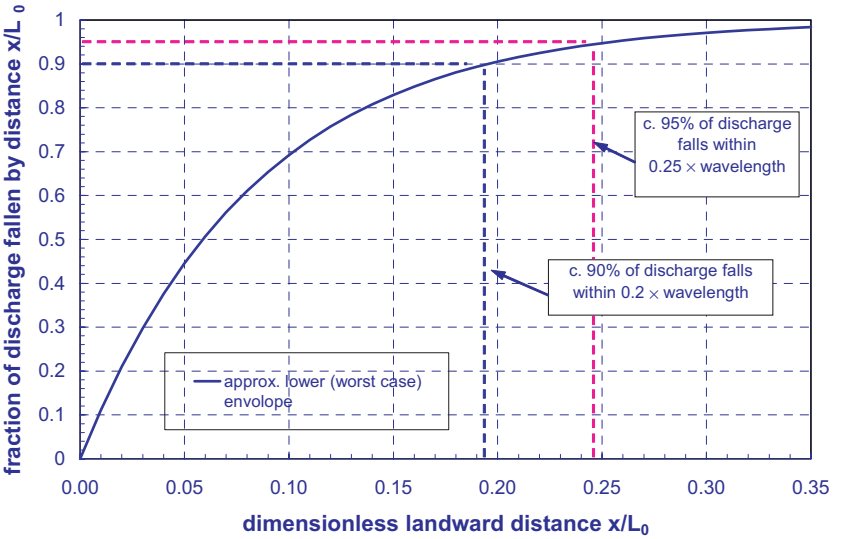

Fig. 16.26. Landward distribution of overtopping discharge under impulsive conditions. Curves show proportion of total overtopping discharge which has landed within a particular distance shoreward of seaward crest.

Under violent (impulsive) overtopping conditions, the idea of spatial extent and distribution has a greater physical meaning — where does the airborne overtopping jet come back to the level of the pavement behind the crest? The answer to this question, however, will (in general) depend strongly upon the local wind conditions.

Despite the difficulty of directly linking a laboratory wind speed to its prototype equivalent (see Sec. 16.3.6), laboratory tests have been used to place an upper bound on the possible wind-driven spatial distribution of the "fall back to ground" footprint of the violently overtopped volumes.[3,17] Tests used large fans to blow air at gale-force speeds (up to 28 m/s) *in the laboratory*. The lower (conservative) envelope of the data (Fig. 16.26) gives the approximate guidance that 95% of the violently-overtopped discharge will land within a distance of $0.25 \times L_o$, where L_o is the offshore (deepwater) wavelength. No data is available for the case of a shallow foreshore with no clear definition of L_o.

16.5.4. *Pressures resulting from downfalling water mass*

Wave impact pressures on the crown deck of a breakwater have been measured in small- and large-scale tests.[19,20] These impacts are the result of an impacting wave at the front wall of the breakwater generating an upward jet which in turn falls back onto the crown deck of the structure. Small-scale tests suggest that local impact pressure maxima on the crown deck are smaller than *but of the same order of magnitude as* wave impact pressures on the front face. For high-crested structures ($R_c/H_{m0} > 0.5$), pressure maxima were observed to occur within a distance of $\sim 1.5 \times H_{m0}$ behind the seaward crest. For lower-crested structures ($R_c/H_{m0} < 0.5$),

this distance was observed to increase to $\sim 2 \times H_{m0}$. Over all small-scale tests, pressure maxima were measured over the range

$$2 < \frac{p_{1/250}}{\rho g H_{m0}} < 17 \quad \text{with a mean value of 8.} \tag{16.27}$$

The largest downfall impact pressure measured in large-scale tests was 220 kPa (with a duration of 0.5 ms). The largest downfall pressures were observed to result from overtopping jets thrown upward by very-nearly breaking waves (the "flip through" condition). Although it might be expected that scaling small-scale impact pressure data would overestimate pressure maxima at large scale, approximate comparisons between small- and large-scale test data suggest that the agreement is good.

Acknowledgments

This chapter was based on the *EurOtop* Overtopping Manual,[14] which was funded in the United Kingdom by the Environmental Agency, in Germany by the German Coastal Engineering Research Council (KFKI), and in the Netherlands by Rijkswaterstaat and Netherlands Expertise Network (ENW) on Flood Protection.

The Project Team for the creation, editing, and support of the manual; the Project Steering Group for guidance and supervision; and a number of individual persons, have been listed and acknowledged in Chap. 14.

References

References have been kept to an absolute minimum. An extensive bibliography can be found in the *EurOtop* Overtopping Manual (2007).

1. N. W. H. Allsop, P. Besley and L. Madurini, Overtopping performance of vertical and composite breakwaters, seawalls and low reflection alternatives, Paper 4.7 in MCS Project Final Report, University of Hannover (1995).
2. P. Besley, Overtopping of seawalls — Design and assessment manual, R&D Technical Report W 178, Environment Agency, Bristol (1999).
3. T. Bruce, T. Pullen, W. Allsop and J. Pearson, How far back from a seawall is safe? Spatial distributions of wave overtopping, *Proc. Int. Conf. Coastlines, Structures and Breakwaters 2005*, ICE London, Thomas Telford (2005), pp. 166–176.
4. T. Bruce, J. Pearson and N. W. H. Allsop, Violent wave overtopping — Extension of prediction method to broken waves, *Proc. Coastal Structures 2003*, ASCE, Reston, Virginia (2003), pp. 619–630.
5. T. Bruce, N. W. H. Allsop and J. Pearson, Hazards at coast and harbour seawalls — Velocities and trajectories of violent overtopping jets, *Proc. 28th Int. Conf. Coastal Eng.*, Cardiff (2002), pp 2216–2226.
6. CEM/H. F. Burcharth and S. A. Hughes, Fundamentals of design, *Coastal Engineering Manual*, eds. L. Vincent and Z. Demirbilek, Part VI, Design of Coastal Project Elements. Chapter VI-5-2, Engineer Manual 1110-2-1100 (US Army Corps of Engineers, Washington, DC, 2002).

7. CLASH, Crest level assessment of coastal structures by full scale monitoring, neural network prediction and hazard analysis on permissible wave overtopping, Fifth Framework Programme of the EU, Contract N. EVK3-CT-2001-00058, www.clash-eu.org.
8. A. Cornett, Y. Li and A. Budvietas, Wave overtopping at chamfered and overhanging vertical structures, *Proc. Int. Workshop on Natural Disasters by Storm Waves and their Reproduction in Experimental Basins*, Kyoto, Japan (1999).
9. J. De Rouck, J. Geeraerts, P. Troch, A. Kortenhaus, T. Pullen and L. Franco, New results on scale effects for wave overtopping at coastal structures, *Proc. Coastlines, Structures and Breakwaters 2005*, ICE London, Thomas Telford (2005), pp. 29–43.
10. L. Franco, M. de Gerloni and J. W. van der Meer, Wave overtopping on vertical and composite breakwaters, *Proc. 24th Int. Conf. Coastal Eng.*, Kobe (1994), pp. 1030–1044.
11. Y. Goda, *Random Seas and Design of Maritime Structures*, 2nd edn. (World Scientific Publishing, Singapore, 2000).
12. A. Kortenhaus, J. Pearson, T. Bruce, N. W. H. Allsop and J. W. van der Meer, Influence of parapets and recurves on wave overtopping and wave loading of complex vertical walls, *Proc. Coastal Structures 2003*, ASCE, Reston, Virginia (2003), pp. 369–381.
13. N. Napp, T. Bruce, J. Pearson and N. W. H. Allsop, Violent overtopping of vertical seawalls under oblique wave conditions, *Proc. 29th Int. Conf. Coastal Eng.*, Cardiff (2002), pp. 4482–4493.
14. Overtopping Manual, *Wave Overtopping of Sea Defences and Related Structures — Assessment Manual*, eds. T. Pullen, N. W. H. Allsop, T. Bruce, A. Kortenhaus, H. Schüttrumpf and J. W. van der Meer (2007), www.overtopping-manual.com.
15. J. Pearson, T. Bruce, N. W. H. Allsop, A. Kortenhaus and J. W. van der Meer, Effectiveness of recurve wave walls in reducing wave overtopping on seawalls and breakwaters, *Proc. 29th Int. Conf. Coastal Eng.*, Lisbon (2004), pp. 4404–4416.
16. J. Pearson, T. Bruce, N. W. H. Allsop and X. Gironella, Violent wave overtopping — Measurements at large and small scale, *Proc. 28th Int. Conf. Coastal Eng.*, Cardiff (2002), pp. 2227–2238.
17. T. Pullen, N. W. H. Allsop, T. Bruce, J. Pearson and J. Geeraerts, Violent wave overtopping at Samphire Hoe: Field and laboratory measurements, *Proc. 29th Int. Conf. Coastal Eng.*, Lisbon (2004), pp. 4379–4390.
18. R. Smid, Untersuchungen zur Ermittlung der mittleren Wellenüberlaufrate an einer senkrechten Wand und einer 1:1,5 geneigten Böschung für Versuche mit und ohne Freibord, Student study at Leichtweiss-Institute for Hydraulics. Braunschweig (2001) (in German).
19. T. Bruce, L. Franco, P. Alberti, J. Pearson and N. W. H. Allsop, Violent wave overtopping: Discharge throw velocities, trajectories and resulting crown deck loading, *Proc. Ocean Wave Measurement and Analysis* ("*Waves 2001*"), ASCE (1999), pp. 1783–1796.
20. G. Wolters, G. Müller, T. Bruce and C. Obhrai, Large scale experiments on wave downfall pressures on vertical and steep coastal structures, *Proc. ICE Maritime Engineering* **158**, 137–145 (2005).